NANOTCAD2D: Two-dimensional code for the simulation of nanoelectronic devices and structures

Gilberto Curatola
Dipartimento di Ingegneria dell'Informazione: Elettronica, Informatica, Telecomunicazioni, Università di Pisa
Giuseppe Iannaccone
Dipartimento di Ingegneria dell'Informazione: Elettronica, Informatica, Telecomunicazioni, Università di Pisa

G. Curatola, G. Iannaccone, "*NANOTCAD2D: Two-dimensional code for the simulation of nanoelectronic devices and structures*", Computational Materials Science, **28**, pp.342-352 (2003).

ELSEVIER

Computational Materials Science 28 (2003) 342–352

COMPUTATIONAL MATERIALS SCIENCE

www.elsevier.com/locate/commatsci

NANOTCAD2D: Two-dimensional code for the simulation of nanoelectronic devices and structures ☆

G. Curatola *, G. Iannaccone

Dipartimento di Ingegneria dell'Informazione, Universitá degli studi di Pisa, Via Diotisalvi 2, I-56122 Pisa, Italy

Abstract

In this paper we present NANOTCAD2D, a code for the simulation of the electrical properties of semiconductor-based nanoelectronic devices and structures in two-dimensional domains. Such code is based on the solution of the Poisson/Schrödinger equation with density functional theory and of the continuity equation of the ballistic current. NANOTCAD2D can be applied to structures fabricated on III–IV, strained-silicon and silicon–germanium heterostructures, CMOS structures, and can easily be extended to new materials. In particular, in the case of SiGe heterostructures, it includes the effects of strain on the energy band profiles. The effects of interface states at the air/semiconductor interfaces, particularly significant in the case of devices obtained with selective etching, are also properly taken into account.

Keywords: Density functional theory; Quantum simulation; Ballistic transport; Nanoscale devices; Nanoelectronics; Nanotechnology computer aided design

1. Introduction

The electrical properties of nanoscale semiconductor devices and structures are typically determined by quantum confinement, that strongly affects the density of states of electrons and holes, and by ballistic transport, that takes place if device length is smaller than the scattering length.

An efficient simulation tool, aimed at understanding device behavior and at designing optimized structures, must therefore include such aspects, and achieve at the same time a reasonable trade-off between efficiency and accuracy.

Here we present NANOTCAD2D, a program for the simulation of nanoelectronic semiconductor devices, based on the self-consistent solution of Poisson/Schrödinger equation and of the continuity equation for electrons and holes in the case of ballistic transport. The program allows to consider quantum confinement in one or two dimensions, and to address more complex structures that can be divided into regions in which different types of confinement are present.

NANOTCAD2D is oriented at two main classes of devices: (i) quantum wires, i.e., structures with translation symmetry in one direction, that are completely described by the geometry of the

☆ Programming language used: FORTRAN 77; computer on which the program has been tested: Linux PCs; memory occupancy in a typical run: 50–100 MB.

* Corresponding author.

E-mail addresses: g.curatola@iet.unipi.it (G. Curatola), g.iannaccone@iet.unipi.it (G. Iannaccone).

0927-0256/$ - see front matter © 2003 Elsevier B.V. All rights reserved.
doi:10.1016/S0927-0256(03)00117-4

cross section; (ii) ballistic field effect devices, again with translation symmetry in a direction perpendicular to that of electron motion.

Ballistic transport is simply included by assuming that the occupation factor of states injected from a given reservoir is that of the reservoir itself, i.e., obeys Fermi–Dirac distribution with reservoir's Fermi energy.

In addition, the code implements a simplified model for localized states at the semiconductor surface exposed to air. Indeed, the depletion of a one-dimensional or a two-dimensional electron gas (1DEG or 2DEG) due to acceptor-like surface states is of primary importance in determining the electrical properties of narrow quantum wires or structures with large exposed surfaces.

At present, the code allows to consider common semiconductor materials, such as silicon, AlGaAs, InGaAs, strained silicon and silicon germanium. In the case of silicon germanium, in particular, we have developed a procedure for taking into account the effect of strain caused by different lattice constants on the band structure [1].

The paper has the following structure: in Section 2 we describe the physical model implemented in the code; in Section 3 we discuss the numerical aspects of the algorithms. In Section 4 simulation examples are presented and in Section 5 the conclusions.

2. Physical model

The density of states for electron and holes depends on the degree of quantum confinement in the different device regions. There are three possibilities: If quantum confinement is strong in both directions, the density of states is obtained by solving the two-dimensional Schrödinger equation. If quantum confinement is strong only in one direction (say, x) the density of states is written as a sum of two-dimensional subbands, the edges of which are obtained by solving the Schrödinger equation in the x direction for each mesh point along the y axis. If confinement can be considered very weak, the density of states of the bulk material is used.

For materials with degenerate or quasi-degenerate minima in the conduction band, such as for example silicon, that has six degenerated minima, the density of states is computed with the effective mass approximation for each minimum, taking into account mass anisotropy. The same procedure is applied to degeneracy of valence band maxima.

In the following, we will discuss in some detail the expressions for the density of states and carrier density considering only one band valley, for simplicity of notation. Extension to multiple valleys is straightforward.

2.1. Charge density for two-dimensional quantum confinement (1DEG–1DHG)

Let us consider a region where the confinement for electrons is strong in both x and y directions. In such a case, the local density of states per unit of volume and energy near a conduction band minimum is given by:

$$N_{1D}(E,x,y) = \frac{\sqrt{2m_z}}{\pi\hbar} \times \sum_i |\Psi_i(x,y)|^2 \times (E - E_i)^{-\frac{1}{2}} u(E - E_i), \tag{1}$$

where $u(E - E_i)$ is the Heavyside function, Ψ_i is the solution of the Schrödinger equation in two dimensions, i.e.,

$$-\frac{\hbar^2}{2m_x}\frac{\partial^2}{\partial x^2}\Psi_i - \frac{\hbar^2}{2m_y}\frac{\partial^2}{\partial y^2}\Psi_i + E_c(x,y)\Psi_i = E_i\Psi_i, \tag{2}$$

E_i is the corresponding eigenvalue, E_c is the conduction band, m_s, $s = x, y, z$ is the effective mass in the direction denoted by the pedix, $\hbar$ is the reduced Planck's constant. At this point, by integrating the density of states multiplied by the Fermi–Dirac occupation factor, the quantum electron density can be expressed as:

$$n = \frac{\sqrt{2m_z k_B T}}{\pi\hbar} \sum_i |\Psi_i|^2 F_{-\frac{1}{2}}\left(\frac{E_f - E_i}{k_B T}\right), \tag{3}$$

where $F_{-1/2}$ is the Fermi–Dirac integral of order $-1/2$ and E_f is the Fermi energy [2].

In order to compute the hole concentration we have to solve Schrödinger equation for heavy holes and for light holes. Therefore, the conduction band in (2) is substituted by the inverted valence

band $-E_v(x,y)$ and the eigenvalues $-E_i^h$, are obtained.

Therefore the hole concentration p becomes:

$$p = \frac{\sqrt{2m_z^h k_B T}}{\pi\hbar} \sum_i |\Psi_i|^2 F_{-\frac{1}{2}}\left(\frac{E_i^h - E_f}{k_B T}\right), \tag{4}$$

where m_z^h is the effective mass for holes in the z direction.

2.2. One-dimensional quantum confinement: two-dimensional electron or hole gas (2DEG–2DHG)

In the case of strong confinement in only one direction (for example along the x axis), we assume that the density of states can be decomposed in a quantum term along the direction of confinement and a semiclassical term in the other directions. The one-dimensional Schrödinger equation for electrons in the x direction for a mesh point y can be written as:

$$-\frac{\hbar^2}{2m_x}\frac{\partial^2}{\partial x^2}\Psi_i + E_c(x,y)\Psi_i = E_i(y)\Psi_i. \tag{5}$$

As a consequence, the available states for electrons are grouped into two-dimensional subbands and the density of states can be expressed as follows:

$$N_{2D}(E,x,y) = \frac{\sqrt{m_y m_z}}{2\pi\hbar^2} \sum_i |\Psi_i(x,y)|^2 u(E - E_i(y)). \tag{6}$$

The electron density therefore is:

$$n = \frac{k_B T\sqrt{m_y m_z}}{\pi\hbar^2} \sum_i |\Psi_i|^2 \ln\left[1 + \exp\left(\frac{E_f - E_i}{k_B T}\right)\right]. \tag{7}$$

Similar considerations apply to holes.

2.3. Effects of surface states

In the simulation of narrow semiconductor devices obtained with selective etching, the effects of states at the exposed surface are very important and must be taken into account in order to reproduce with accuracy the experimental results. In particular, these states can act as donors or acceptors and hence deeply affect the carrier distribution in the device.

In order to correctly model the phenomenon, we have used a simple model based on two parameters that is typically applied to metal-semiconductor contacts [3] and has been recently validated for air-semiconductor interfaces [4].

The two parameters are the density of interface states per unit energy per unit area D_S [$eV^{-1}\,cm^{-2}$] and the energy difference Φ^* between the vacuum level E_0 and the Fermi energy that ensures a neutral charge at the interface. States with energy below $E_0 - \Phi^*$ are donors and states with higher energy are acceptors.

Surface charge per unit surface can then be expressed as $Q_s = -qD_S[E_f - (E_0 - \Phi^*)]$, where $-q$ is the electron charge.

2.4. Poisson equation

All charge concentrations considered represent the source term of the two-dimensional Poisson equation:

$$\begin{aligned}\nabla\cdot(\epsilon\nabla\Phi) &= -\rho[\Phi] \\ &= -q[-n[\Phi] + p[\Phi] + N_D^+[\Phi] \\ &\quad - N_A^-[\Phi] + \rho_s[\phi]],\end{aligned} \tag{8}$$

where ϵ is the dielectric constant, q is the electron charge, ρ_s is the term of surface charge per unit volume, N_D^+ and N_A^- the ionized donor and acceptor concentrations, respectively [3]. Energy bands depend on the potential as:

$$\begin{aligned}E_c(x,y) &= E_c(x,y)|_{\Phi=0} - q\Phi(x,y), \\ E_v(x,y) &= E_v(x,y)|_{\Phi=0} - q\Phi(x,y).\end{aligned} \tag{9}$$

Potential and charge density profiles in equilibrium are computed by solving the set of nonlinear partial differential equations described above. The case of ballistic transport is examined in the next section.

2.5. Ballistic transport for electrons and holes

When carriers are injected into a semiconductor device, they are likely to be scattered by a number of possible sources, including acoustic and optical phonons, ionized impurities, defects, interfaces

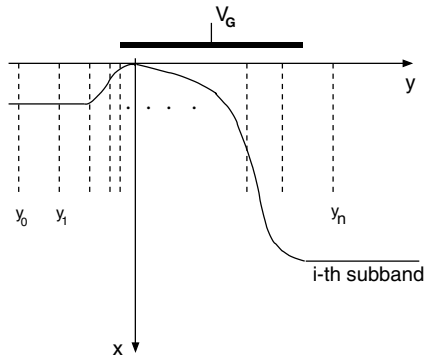

Fig. 1. Energy profile along the channel for a nanoscale FET. Only electrons with energy higher than the barrier peak contribute to the current.

and other carriers. If, however, device length is smaller than the mean free path it is very likely for carriers to traverse the device without suffering scattering events. Our code includes this type of "ballistic" transport.

Ballistic transport is implemented here only in the case of one-dimensional quantum confinement, when a description in terms of two dimensional subbands is used. Indeed, we have shown that such assumption involves a negligible error also in devices with channel length down to 25 nm [5].

Let us consider Fig. 1, representing a subband profile for electrons along the channel. Carriers are injected into the channel from a reservoir (source) and contribute to the current only if they overcome the barrier modulated by the gate voltage and, to a lesser degree, by the drain voltage (DIBL).

If we neglect the interaction between electrons and ions and among electrons, we can simply assume that electrons with injected longitudinal energy lower than the subband maximum are reflected back to their originating contact, while the others are transmitted over the barrier and contribute to the current [6,7].

Therefore, for each subband we evaluate the subband maximum $E_{i\max}$ and the corresponding longitudinal position $y_{i\max}$. All electrons with longitudinal energy lower than $E_{i\max}$ are in equilibrium with the originating contact, while electrons with longitudinal energy higher than $E_{i\max}$ conserve the chemical potential of the injecting reservoir. The occupation factor f is therefore:

$$f(E,E_{\mathrm{F}}) = \begin{cases} \left[1+\exp\left(\frac{E-E_{\mathrm{FS}}}{k_{\mathrm{B}}T}\right)\right]^{-1} \\ \quad \text{if } y < y_{i\max},\ E < E_{i\max}, \\ \left[1+\exp\left(\frac{E-E_{\mathrm{FD}}}{k_{\mathrm{B}}T}\right)\right]^{-1} \\ \quad \text{if } y > y_{i\max},\ E < E_{i\max}, \\ \left[1+\exp\left(\frac{E-E_{\mathrm{FS}}}{k_{\mathrm{B}}T}\right)\right]^{-1} + \left[1+\exp\left(\frac{E-E_{\mathrm{FD}}}{k_{\mathrm{B}}T}\right)\right]^{-1} \\ \quad \text{if } E > E_{i\max}, \end{cases} \tag{10}$$

where E_{FS} (E_{FD}) is the source (drain) Fermi energy. If we write the total energy E as $E = E_y + E_z$, where the term $E_y = E_i + \frac{\hbar^2 k_y^2}{2m_y}$ is the longitudinal energy, and $E_z = \hbar^2 k_z^2/2m_z$ the transverse energy, the density of states reads:

$$N_{2\mathrm{D}}(E_y,E_z)\,\mathrm{d}E = 2\sum_i |\Psi_i|^2 \frac{\sqrt{m_y m_z}}{h^2}\frac{1}{\sqrt{E_y E_z}}\,\mathrm{d}E_y\,\mathrm{d}E_z, \tag{11}$$

and the electron density is accordingly given by:

$$n = \int_0^{E_{i\max}-E_i(y)} \sum_i |\Psi_i|^2 2\frac{\sqrt{m_y m_z}}{h^2} E_y^{-\frac{1}{2}}\,\mathrm{d}E_y \times \int_0^{\infty} E_z^{-\frac{1}{2}} f(E,E_{\mathrm{F}})\,\mathrm{d}E_z. \tag{12}$$

The electron current is evaluated assuming that there is no tunnel current through the barrier so that only the electrons with longitudinal energy higher than $E_{i\max}$ can contribute.

$$J_n = \int_0^{\infty}\mathrm{d}E_z \int_{E_{i\max}-E_i(y)}^{\infty} \sum_i 2\frac{\sqrt{m_y m_z}}{h^2}\frac{1}{\sqrt{E_y E_z}}\sqrt{\frac{2E_y}{m_y}} \times \left[\frac{1}{1+\exp\left(\frac{E_y+E_z-E_{\mathrm{FS}}}{k_{\mathrm{B}}T}\right)} - \frac{1}{1+\exp\left(\frac{E_y+E_z-E_{\mathrm{FD}}}{k_{\mathrm{B}}T}\right)}\right]\mathrm{d}E_y. \tag{13}$$

Similar considerations apply to holes.

3. Numerical aspects

The flow diagram of the algorithm implemented is shown in Fig. 2. The program, using an initial guess for the potential, starts with a semiclassical solution of the Poisson equation. The equation is discretized with the box-integration method and solved with the Newton–Raphson algorithm. Dirichlet boundary conditions are enforced on each metal gate and homogeneous Neumann conditions on the rest of the domain boundary. The solution obtained is used as an initial guess for the quantum calculation, where the nested Poisson/Schrödinger equation must be solved.

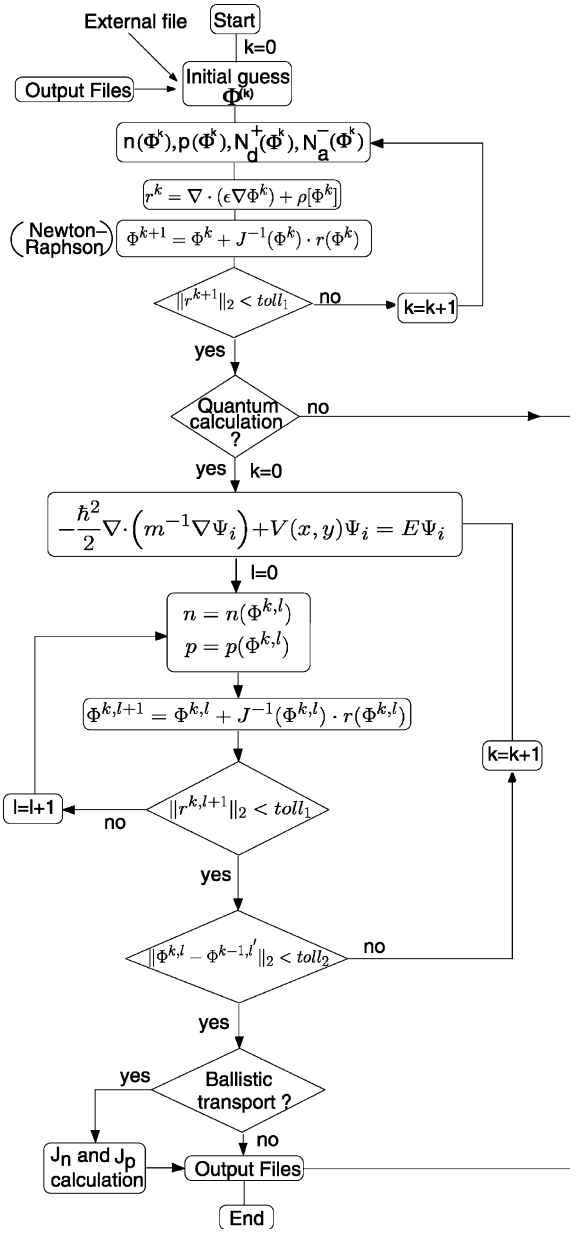

Fig. 2. Flow diagram of the algorithm implemented.

In order not to degrade convergence speed of the algorithm when also the Schrödinger equation has to be solved, we have implemented a simplified version of the predictor-corrector scheme proposed in Ref. [8]. In this way, instead of solving both equations at each Newton–Raphson step, we evaluate eigenfunctions and eigenvalues only at the beginning of a Newton–Raphson cycle: for a whole cycle eigenfunctions and the difference between the eigenvalues and the energy bands in each point of the domain are assumed to be constant. When a Newton–Raphson cycle ends the Schrödinger equation is solved again and a new cycle is started. The program ends when the difference between the two-norm of the potential at the end of two successive Newton–Raphson cycles is lower then a fixed tolerance [9].

In Fig. 3(left) a rectangular uniform mesh is shown, where it is possible to notice to the subdomain $D_{i,j}$ (dashed line) associated to the generic grid point (i,j). In our code, we have divided the properties of the structure in *point* characteristics and *material* characteristics.

Point characteristics are, for example, the potential, the Fermi level, charge concentrations, while material properties (e.g., energy gap, electron

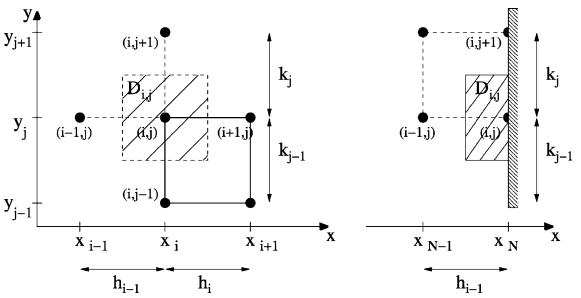

Fig. 3. $D_{i,j}$ represents the region associated to the grid point (i,j). In the figure the case of an internal point (left) and of a boundary point (right) are shown.

affinity, etc.) belong to the second group. In the figure, is also shown (solid line) the material element connected to the generic (i,j) grid point.

In each subdomain, Poisson and Schrödinger equations are discretized with box-integration [10].

3.1. Poisson equation

In particular, for the Poisson equation, after integrating both membersover the domain $D_{i,j}$, we obtain:

$$\int\int_{D_{i,j}} \nabla\cdot(\epsilon\nabla\Phi(x,y))\,\mathrm{d}x\,\mathrm{d}y = -\int\int_{D_{i,j}} \rho(x,y)\,\mathrm{d}x\,\mathrm{d}y, \tag{14}$$

which is discretized as

$$\begin{aligned}
&\frac{\Phi_{i+1,j}-\Phi_{i,j}}{h_i}\left[\epsilon_{i,j+1}\frac{k_j}{2}+\epsilon_{i,j}\frac{k_{j-1}}{2}\right]\\
&+\frac{\Phi_{i,j+1}-\Phi_{i,j}}{k_j}\left[\epsilon_{i,j+1}\frac{h_i}{2}+\epsilon_{i-1,j+1}\frac{h_{i-1}}{2}\right]\\
&-\frac{\Phi_{i,j}-\Phi_{i-1,j}}{h_{i-1}}\left[\epsilon_{i-1,j+1}\frac{k_j}{2}+\epsilon_{i-1,j}\frac{k_{j-1}}{2}\right]\\
&-\frac{\Phi_{i,j}-\Phi_{i,j-1}}{k_{j-1}}\left[\epsilon_{i,j}\frac{h_i}{2}+\epsilon_{i-1,j}\frac{h_{i-1}}{2}\right]\\
&=\Big[-q(p_{i,j}-n_{i,j}+N^+_{\mathrm{D}i,j}-N^-_{\mathrm{A}i,j})\\
&\quad+\rho_{fi,j}\Big]\frac{(h_i+h_{i-1})(k_j+k_{j-1})}{4},
\end{aligned} \tag{15}$$

where $h_i = x_{i+1}-x_i$, $k_j = y_{j+1}-y_j$, and pedices i, j denote the quantity in position (x_i,y_j).

Proper boundary conditions must be enforced to the equation, such as Dirichlet boundary conditions on each metal gate and homogeneous Neumann conditions on the rest of the domain boundary. In the first case, the potential Φ is fixed, while in the second case, the electric field $\vec{\nabla}\Phi\cdot\vec{n}=-\varepsilon$ is fixed.

In the simulation code, we have chosen as reference level for energies the vacuum level E_0 and hence the potential for each gate point is obtained as:

$$\Phi i,j = E_0 - \phi^n_{\mathrm{work}} - E^n_{\mathrm{F}}, \tag{16}$$

where E^n_{F} and ϕ^n_{work} represent the Fermi level and the work function of the nth gate, respectively.

Let us consider a point (i,j) on the boundary and let us make reference to the Fig. 3(right): observe how the region $D_{i,j}$ is much smaller with respect to the case of internal point ($D_{i,j}$ becomes a quarter in the case of each of four vertexes grid points). In this point, we enforce Neumann condition and the discretization of the Poisson equation becomes:

$$\begin{aligned}
&\varepsilon\left[\epsilon_{i,j+1}\frac{k_j}{2}+\epsilon_{i,j}\frac{k_{j-1}}{2}\right]\\
&\quad+\frac{\Phi_{i,j+1}-\Phi_{i,j}}{k_j}\left[\epsilon_{i-1,j+1}\frac{h_{i-1}}{2}\right]\\
&\quad-\frac{\Phi_{i,j}-\Phi_{i-1,j}}{h_{i-1}}\left[\epsilon_{i-1,j+1}\frac{k_j}{2}+\epsilon_{i-1,j}\frac{k_{j-1}}{2}\right]\\
&\quad-\frac{\Phi_{i,j}-\Phi_{i,j-1}}{k_{j-1}}\left[\epsilon_{i-1,j}\frac{h_{i-1}}{2}\right]\\
&\quad=\Big[-q\Big(p_{i,j}-n_{i,j}+N^+_{\mathrm{D}i,j}-N^-_{\mathrm{A}i,j}\Big)\\
&\qquad+\rho_{fi,j}\Big]\frac{(h_{i-1})(k_j+k_{j-1})}{4}.
\end{aligned} \tag{17}$$

3.2. Schrödinger equation

The two-dimensional single-particle Schrödinger equation for electrons, given a conduction band profile $E_{\mathrm{c}}(x,y)$, reads:

$$-\frac{\hbar^2}{2}\nabla\cdot[m^{-1}\nabla\Psi_n]+E_{\mathrm{c}}(x,y)\Psi_n = E_n\Psi_n, \tag{18}$$

where $\Psi_n(x,y)$ represents the nth eigenfunction, E_n is the nth eigenenergy, m is the electron effective mass tensor in the plane perpendicular to the direction of propagation,

$$m=\begin{bmatrix} m_x & 0\\ 0 & m_y\end{bmatrix}. \tag{19}$$

In our simulations, we have discarded the exchange-correlation term, since it provides a very small contribution. Dirichlet boundary conditions are enforced on the quantum simulation domain [11].

With the box-integration method, we obtain:

$$
\begin{aligned}
&-\frac{\hbar^2}{4}\left[\frac{\Psi_{n_{i+1,j}}-\Psi_{n_{i,j}}}{h_i}\left[\frac{k_j}{m_{x_{i,j+1}}}+\frac{k_{j-1}}{m_{x_{i,j}}}\right]\right]\\
&-\frac{\hbar^2}{4}\left[\frac{\Psi_{n_{i,j+1}}-\Psi_{n_{i,j}}}{k_j}\left[\frac{h_i}{m_{y_{i,j+1}}}+\frac{h_{i-1}}{m_{y_{i-1,j+1}}}\right]\right]\\
&+\frac{\hbar^2}{4}\left[\frac{\Psi_{n_{i,j}}-\Psi_{n_{i-1,j}}}{h_{i-1}}\left[\frac{k_j}{m_{x_{i-1,j+1}}}+\frac{k_{j-1}}{m_{x_{i-1,j}}}\right]\right]\\
&+\frac{\hbar^2}{4}\left[\frac{\Psi_{n_{i,j}}-\Psi_{n_{i,j-1}}}{k_{j-1}}\left[\frac{h_i}{m_{y_{i,j}}}+\frac{h_{i-1}}{m_{y_{i-1,j}}}-\right]\right]\\
&+E_{c_{i,j}}\Psi_{n_{i,j}}\frac{(h_i+h_{i-1})(k_j+k_{j-1})}{4}\\
&=E_n\Psi_{n_{i,j}}\frac{(h_i+h_{i-1})(k_j+k_{j-1})}{4}. \qquad (20)
\end{aligned}
$$

3.3. Numerical routines and performance

The discretized non-linear Poisson equation is solved with the Newton–Raphson (NR) algorithm. The sparse system of linear algebraic equations of each NR step is solved with the package Y12MAF [12], which is based on Gaussian elimination.

The eigenvalue problem resulting from the discretization of the Schrödinger equation in one dimension it is solved with the routine TQLI [12], while in two dimensions is solved with the method proposed in Ref. [11] that allows to reduce computing time without significant loss in accuracy, by solving the problem in the momentum space. The method can be applied to structures with inhomogeneous effective mass and can easily be extended to the full band structure.

The computing time on an 1800 MHz Pentium IV CPU strongly depends on the type of simulation: In the case of quantum confinement in one direction the CPU running time for a 128×61 grid is 37.14 s, while in the case of quantum confinement in two directions, with a 113×148 point grid, the CPU running time is about 95.44 s. These results represent the worst case, with no initial guess of the unknown potential. Finally, in the case of a simulation of ballistic current the running time is strongly affected by the initial guess of the potential and is between a few minutes and an hour. The initial guess is also very important in order to avoid convergence problems of the algorithm.

4. Examples of simulation

In this section, two examples of simulations computed on nanoscale devices are shown. The first structure is a silicon–germanium high mobility electron waveguide schematically represented in Fig. 4. It consists of a $Si_{0.8}Ge_{0.2}$ virtual substrate, an 11 nm strained-silicon layer in which the 1DEG forms, a 5.7 nm undoped $Si_{0.8}Ge_{0.2}$ spacer layer, a 5.7 nm $Si_{0.8}Ge_{0.2}$ doped layer, with $N_d = 10^{18}$ cm^{-3}, a 35 nm undoped $Si_{0.8}Ge_{0.2}$ spacer and a 15 nm undoped silicon cap layer. The second spacer is rather thick, in order to prevent the formation of another electron channel in the silicon cap layer. The waveguide is 160 nm wide [1,13]. Finally, we assume that a triple metal gate is deposited over the structure forming a Schottky contact. For the purpose of our simulation, the Schottky junction is reverse-biased and assumed to be perfectly insulating.

Quantum confinement of carriers in the horizontal (y) direction is provided by selective etching and by the depletion region induced by acceptor states at the exposed surfaces. This last

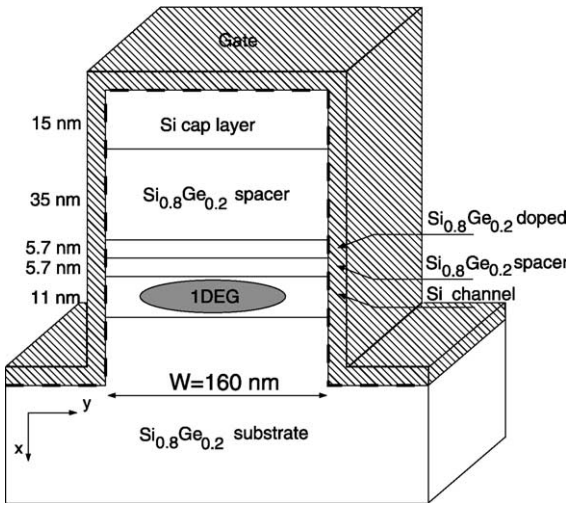

Fig. 4. Silicon–germanium etched electron waveguide.

effect causes the electrical width of wire to be significantly smaller then the etched width. Along the growth (x) direction, as a consequence of the band alignment between strained-silicon and silicon–germanium, a quantum well for electrons forms. In particular, the strained silicon channel is grown under a tensile strain and thus two valleys of the conduction band, along k_x, are lowered in energy while the other four valleys are raised. This condition is required in order to obtain a confinement region for electrons. In addition, only the two lowest conduction band valleys are occupied and the energy splitting between valleys (120 meV) leads to strongly suppressed intervalley scattering.

The self-consistent Poisson/Schrödinger equation is discretized onto a non-uniform rectangular grid of 108×137 points and the electron concentration has been calculated by solving the Schrödinger equation inside the strained silicon channel. Quantum electron density is represented in Fig. 5, where it is possible to observe how the electrical waveguide width is about 95 nm, instead of 160 nm, because of the electron depletion induced by interface states at the exposed surfaces. By tuning the voltage applied to the gate, it is possible to vary the electron density in the channel and hence the number of occupied states. Thus, referring to the Landauer formula of the quantized conductance $G = N(2e^2/h)$ with N equal to the number of propagating modes, it is possible to vary, as a function of applied voltage, the quantum conductance in the channel, as shown in Fig. 6.

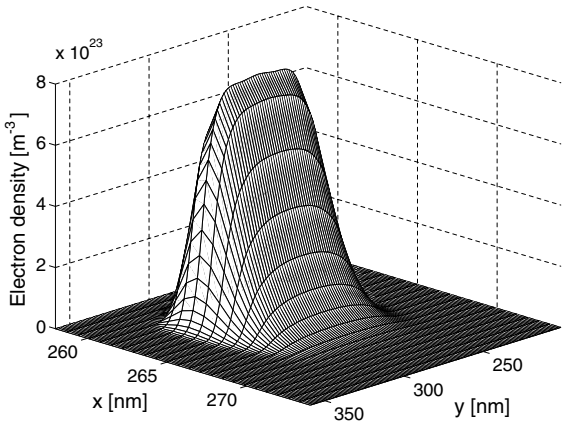

Fig. 5. Quantum electron density in the strained silicon channel of the electron waveguide.

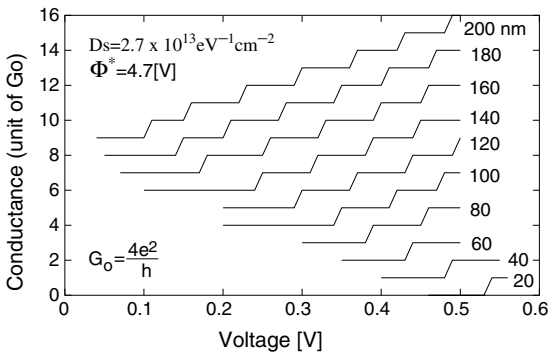

Fig. 6. The voltage applied to an external gate allows us to select the number of propagating modes in the waveguide. The conductance is plotted as a function of the gate voltage for several etched widths of the wire. For presentation clarity each curve is shifted by one conductance quantum.

The second simulation example refers to a "well tempered" ballistic MOSFET with channel length of 25 nm, proposed by Antoniadis et al. [14] and schematically represented in the inset of Fig. 7. The oxide thickness is 1.5 nm and the polysilicon gate has a donor concentration of 5×10^{20} cm^{-3}. In order to reduce short channel effects a super-halo doping is implanted in the channel. The analytic doping profile can be found in Ref. [14].

Assuming fully ballistic transport in the channel, we have computed the source-to-drain current.

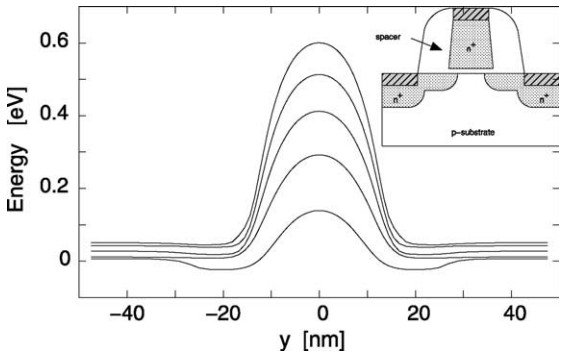

Fig. 7. Subband energies corresponding to a gate voltage of 1 V and a drain voltage 0 V. The transmission coefficient through the barrier is assumed to be unity for electrons with energy higher than the peak of the barrier and zero for electron with energy lower than the peak.

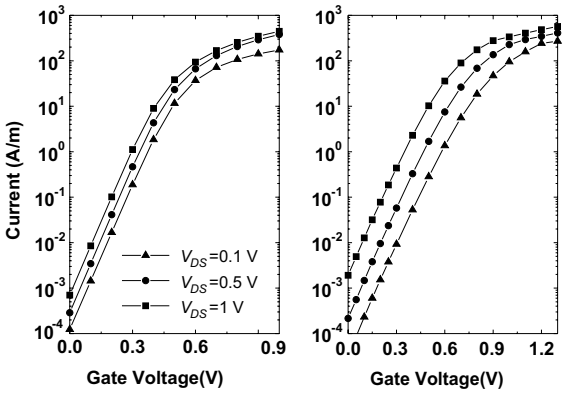

Fig. 8. Transfer characteristics of the 25 nm MOSFET computed with MEDICI (left, from Ref. Antoniadis) and with NANOTCAD2D (right).

The energy barrier that electrons encounter traveling from the source towards the drain is represented in Fig. 7 for a gate voltage $V_{GS} = 1$ V and drain-to-source voltage $V_{DS} = 0$ V. Only the first five subbands are shown. Quantum tunneling has not be considered in our model and therefore the transmission coefficient is unity above the peak of the barrier and zero below. Thus, only electrons with energy higher than the peak can traverse the channel without energy loss and contribute to the total current.

The transfer characteristics obtained with the MEDICI simulator and with NANOTCAD2D are compared in Fig. 8.

The two-dimensional simulator is available, after registration, at the URL: http://www.phantomshub.com. In the directory NANOTCAD2D it is possible to find additional examples of nanoscale semiconductor devices, among which users can find two different types of high mobility electron waveguides defined by selective etching on a SiGe heterostructures, a nanoscale ballistic silicon MOSFET and a nanoscale ballistic AlGaAs field effect transistor (Fig. 9). The parameters of simulation can be varied according to the specific user requirements. In particular, input files can be modified by user directly via a web interface as an HTML form or uploaded from an external source (Fig. 10). In the same directory it is also possible to find a detailed tutorial regarding the input data files structure.

Finally, the hub provides basic visualization capabilities for 2D and 3D plots controlled via a web interface (Fig. 11).

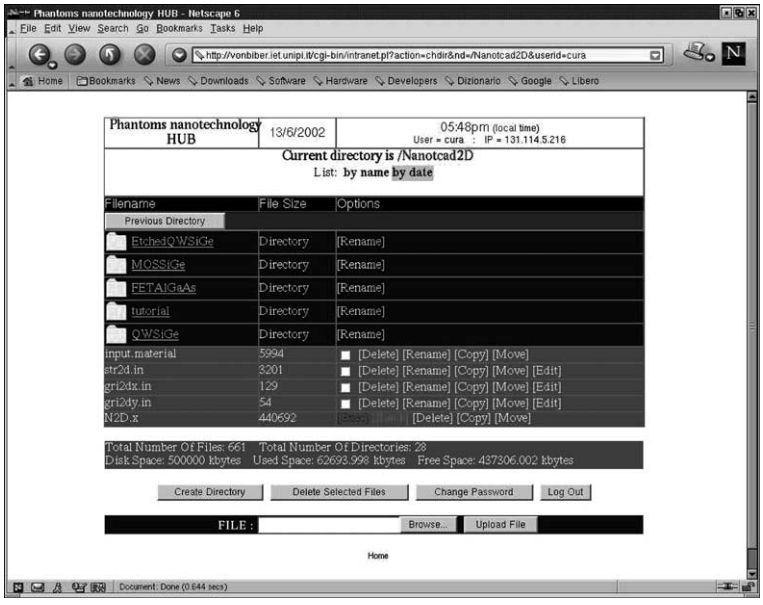

Fig. 9. Screen shot of the user page with the list of simulation examples of NANOTCAD2D.

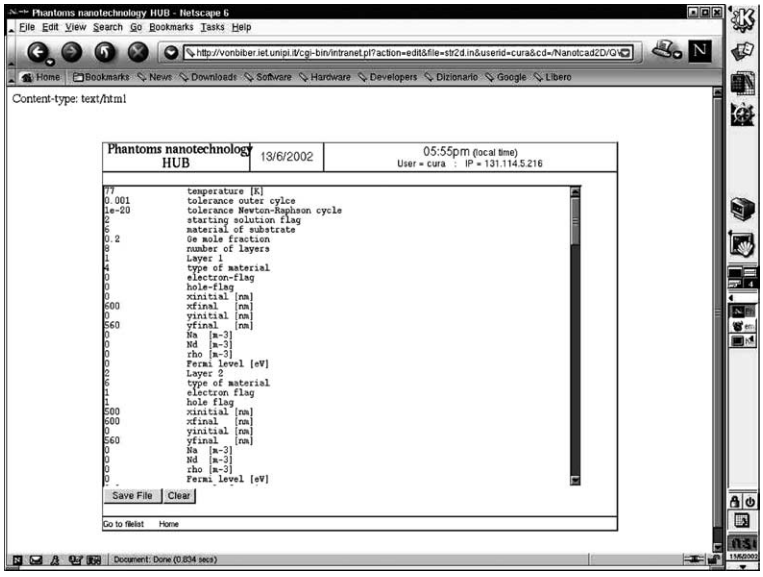

Fig. 10. The parameters of simulation can be varied in accordance with the specific user requirements via an html form.

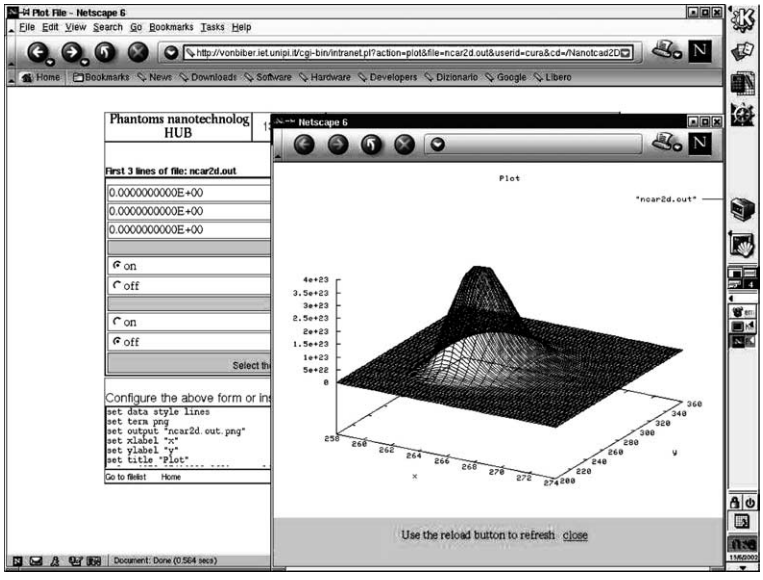

Fig. 11. Basic visualization capabilities are available to the user via a web interface.

5. Discussion and future developments

In this paper we have presented a two dimensional quantum simulator based on the solution of the Poisson/Schrödinger equation with the box-integration method. The code solves also the continuity equation for electrons and holes in the case of ballistic transport, where propagating

states are populated according to the occupation factor of the originating reservoir. NANOTCAD2D allows to simulate most common semiconductors, such as silicon, AlGaAs, InGaAs, strained silicon and silicon germanium and has been successfully used to simulate III–IV heterostructures, strained-silicon and silicon germanium heterostructures, CMOS structures. In the case of silicon–germanium based devices a dedicated procedure allows to take into account the effects of strain on the energy bands and on band alignment.

Next extensions of the models implemented include full two-dimensional quantum transport and quantum tunneling, that becomes relevant for devices with channel length shorter than 10 nm. In addition, we are developing a model for quasi-ballistic transport, which accounts for the possibility that a fraction of carriers undergo elastic scattering, that would allow a more accurate simulation of nanoscale field effect transistor at room temperature.

References

[1] G. Curatola, G. Iannaccone, Nanotechnology 13 (2001) 267.
[2] A. Trellakis, A.T. Galick, U. Ravaioli, Solid State Electron. 41 (1997) 771.
[3] S.M. Sze, Physics of Semiconductor Devices, John Wiley, New York, 1981.
[4] M.G. Pala, G. Iannaccone, S. Kaiser, A. Schliemann, L. Worschech, A. Forchel, Nanotechnology 13 (2002) 373.
[5] G. Fiori, G. Iannaccone, Nanotechnology 13 (2002) 294.
[6] K. Natori, J. Appl. Phys. 76 (1994) 4879.
[7] M. Lundstrom, R. Zhibin, IEEE Trans. Electron Dev. 49 (2002) 113.
[8] A. Trellakis, A.T. Galick, A. Pacelli, U. Ravaioli, J. Appl. Phys. 81 (1997) 7880.
[9] A. Trellakis, U. Ravaioli, J. Appl. Phys. 86 (1999) 3911.
[10] S. Selbeherrer, Analysis and Simulation of Semiconductor Devices, Springer-Verlag Wien, New York, 1984.
[11] M.G. Pala, G. Iannaccone, Nanotechnology 13 (2002) 369.
[12] Freely downloadable from <www.netlib.org>.
[13] G. Curatola, G. Iannaccone, J. Appl. Phys., submitted for publication.
[14] D.A. Antoniadis, I.J. Djomehri, K.M. Jackson, S. Miller. Available from <http://www-mtl.mit.edu/Well/>, 1999.